Journal of Molecular Liquids 427 (2025) 127449

Contents lists available at ScienceDirect

Journal of Molecular Liquids

journal homepage: www.elsevier.com/locate/molliq

Thermal dynamics and magnetohydrodynamics in ferrofluidic wall jet flow: Entropy generation in heat and mass transfer

S.M. Sachhin [a], U.S. Mahabaleshwar [a,*], N. Swaminathan [b], L.M. Pérez [c], Junye Wang [d,*]

[a] Department of Studies in Mathematics, Davangere University, Shivagangothri, Davangere 577 007, India
[b] Engineering Department, Cambridge University, Cambridge CB2 1PZ, UK
[c] Departamento de Ingeniería Industrial y de Sistemas, Universidad de Tarapacá, Casilla 7D, Arica 1000000, Chile
[d] Faculty of Science and Technology, Athabasca University, 1 University Drive, Athabasca, Alberta T9S 3A3, Canada

ARTICLE INFO

Keywords:
Ferro-nanofluid
Entropy generation
Hybrid nanofluids
Brownian motion
Thermophoretic parameter

ABSTRACT

Wall jet nanofluids with entropy generation possess several applications in cooling electronic devices, and solar collectors. The unique magnetic properties of the ferro-nanoparticles allow for the precise control of fluid flow using external magnetic fields, which is invaluable for targeted cooling or heating. In this study, we investigate wall jet hybrid nanofluid materials with ferrous-ferric oxide and copper oxide in conventional fluid water. The governing velocity, mass, and heat transfer equations are calculated to a set of ordinary differential equations (ODEs) via similarity parameters that are solved numerically. Effects of physical parameters, including thermophoretic parameters, Brownian motion parameters, and magnetic parameters, on velocities, temperature and entropy generations are analyzed using graphical representations. The results show that rising the Brownian motion, the magnetic term, or the thermophoresis term rises the fluid temperature. Furthermore, Brownian motion, or the thermophoresis effect increases temperature more for the ferro-hybrid nanofluids than that for single nanofluid. Increasing the thermophoretic parameters and Brown motion lead to the decay of the entropy generation due to enhanced thermal gradients and particle movement. However, the entropy generation enhances as the thermal radiation term rises. This demonstrates that the hybrid nanofluids can raise the thermal and mass transfer but no effects on velocities and entropy generation, compared to the single nanofluid.

1. Introduction

Wall jet ferro-hybrid nanofluids with entropy generation can significantly enhance thermal conductivity and efficiency of energy systems in electronics and microelectronics cooling applications [1–4]. Aly et al. [1] studied wall jet flow and energy influence on hybrid nanofluid flow with injection/suction. Their results showed that rise in radiation resulted in the enhanced thermal boundary for water-Al_2O_3-Cu nanofluids. Usafzai et al. [2] explored wall jet nanofluid movement with thermal energy with power-law velocity. Sachhin et al. [3] analysed heat exchange influence on hybrid nanofluid flow across stretching sheet. Their results showed that the choice of skin friction for wall jet movement at the sheet decays by higher than 50 % when the magnetic field applied. Usafzai et al. [4] evaluated wall jet fluid movement and energy transfer with commonly examined nanoparticles; namely titanium oxide, alumina, copper, and silver. They found that the movement of alumina has similar performance as titanium oxide while copper has similar performance as silver. Nanoparticle's concentration could significantly affect thermal boundary layer, leading to energy uplift, while the injection causes a decay in thermal boundary.

Ferro-hybrid nanofluids are made of ferrous materials and represent a significant advancement in fluid dynamics and heat transfer due to their enhancement in stability, responsiveness, and magnetic performance. The unique magnetic properties of the ferro-nanoparticles allow for the precise control of fluid flow using external magnetic fields, which is invaluable for targeted cooling or heating [5]. Moreover, the ability to manipulate these fluids using magnetic fields opens up new possibilities in microfluidic devices and targeted drug delivery systems. Therefore, ferro nanofluids and hybrid nanofluids are utilized for the thermal transfer of the fluid movement by using a magnetic field, Peclet number, and heat flux effects [6–8]. Sachhin et al. [9] analysed heat transfer influence on hybrid nanofluid movement across stretching surface. They

* Corresponding authors.
E-mail addresses: sachinsm030@gmail.com (S.M. Sachhin), u.s.m@davangereuniversity.ac.in (U.S. Mahabaleshwar), ns341@eng.cam.ac.uk (N. Swaminathan), lperez@academicos.uta.cl (L.M. Pérez), junyew@athabascau.ca (J. Wang).

https://doi.org/10.1016/j.molliq.2025.127449
Received 19 October 2024; Received in revised form 20 March 2025; Accepted 22 March 2025
Available online 23 March 2025

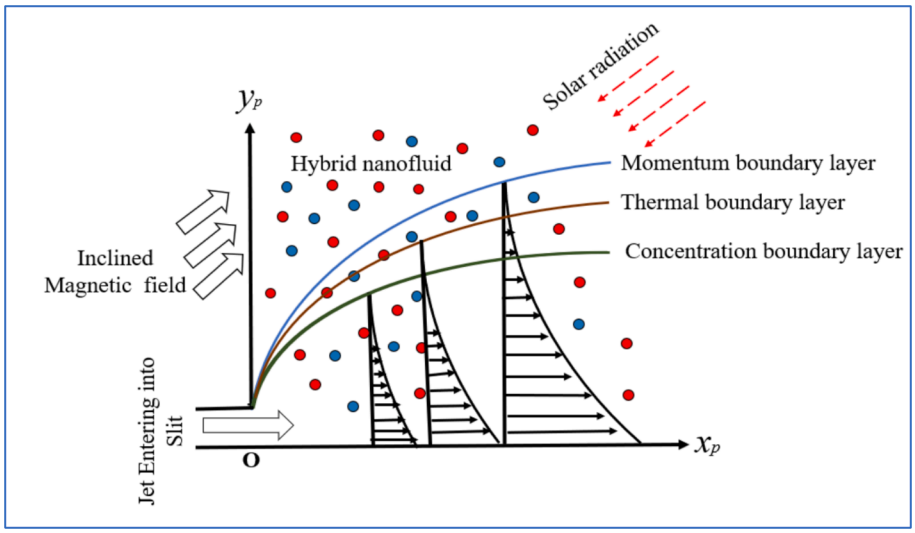

Fig. 1. Physical diagram of the fluid movement.

found that the momentum increased as the thermal radiation term and the volume fraction of a nanoparticle enhanced, but inverse effects for the magnetic term and the Weissenberg parameter. Ahmed et al. [10] performed energy analysis on Ferro fluid movement via radiated Riga plate. Their results showed that enhancing radiation parameter increases the temperature. Casson term reduces the transverse and axial velocity of the fluid. Sachhin et al. [11] examined an impact of slip-on Hiemenz stagnation movement of ternary nanofluid. They found that the magnetic term rises temperature but decays the fluid movement.

Ferro-hybrid nanofluids have advantages of reduced entropy generation and higher exergy efficiency but disadvantages of lower heat transfer coefficients, compared to conventional nanofluids. Entropy generation can be used to identify energy losses and irreversibility of a system, thereby providing insights into how to optimize system performance and energy conservation efficiency. For instance, in heat transfer applications, minimizing entropy generation can lead to more efficient thermal systems. By reducing the entropy generation, engineers can design systems that not only save energy but also reduce the environmental impact. [12–15] explored the effects of various types of thermal radiation on fluid flow across different boundaries. They found that thermal radiation enhanced entropy generation. The entropy generation of cooling liquid with a heat source and the operation of a microprocessor was analysed due to heat flux and found that the heat source raises the entropy generation [16,17]. In engineering and physics, the magnetic fields have been used for manipulation of fluid flow in cooling systems of nuclear reactors and the targeted delivery of drugs in biomedical applications. The importance of magnetic fields in fluid flow is not only for optimizing fluid movement and thermal transfer in large-scale industrial applications but also those in micro-magneto fluidics. [18–21] studied the magnetic field impact on non-Newtonian fluids movement over various boundaries. [22–35] explored the influence of volume fraction and magnetic field on fluid flow via expanding surfaces. Xu et al. [36] studied the energy conversion and magnetic field influence on fourth-grade fluid flow. Khan et al. [37] studied the numerical analysis on graphene nanofluid flow with influence of velocity slip. Nazeer et al. [38] explored the different phase flows of third-grade fluid by using Hafnium nano particles. Qian et al. [39] examined the skin friction analysis of the fluid movement across curved expanding sheet. Khan et al. [40] examined the rheological examination of Eyring Powell nanofluid in porous media. Guo et al. [41] explored the simulations of magnetic force and ramped energy profile on the fluid movement over permeable sheet. Das et al. [42,43] studied the thermal radiation effect on couple stress model across expanding surface. They found that the velocity profile decays due to a magnetic field and slip condition. Ali et al. [44,45] examined the Hall current and slip effects on convective movement across exponential expanding sheet. Adhikari and Das [46] studied the Casson fluid movement across cylindrical sheet with entropy production. Their results showed that Lorentz force and porosity reduces fluid flow. Karmakar et al. [47] examined the heat exchange and Darcian effect on fluid movement across Oscillating surface. Yadav et al. [48,49] explored the impact of magnetic field on convective nanofluid layer. Alipour et al. [50,51] and Akbari et al. [52] utilized the porous medium to theoretically analyses the fluid movement. They found that the nanoparticle shape factor could significantly affect the heat transfer. Kausar et al. [53] studied the heat exchange impact on Casson fluid movement through chemical reaction. Yadav et al. [54] explored the cellular convective Casson fluid flow in a porous layer. They found that the viscosity disparity influences the convective movement. Zangooee et al. [55] studied 3-dimensional fluid flow under MHD on exponential expanding/shrinking plate. Their results showed that the shape factor enhances the temperature. Moghimi et al. [56] explored the magnetic field impact on the fluid movement via expanding surface. Their results showed that the dimensionless maximum velocity reduced by 10.7 % when Hartmann number raises from 0 to 5. Mahboobtosi et al. [57] explored the shape factor influence on ternary and single nanofluid movements cross expanded cylinder. [58–64] studied the thermal radiation effect on different fluid models across various boundaries. Their results revealed that magnetic field enhances the skin friction of the fluid flow. However, ferro-hybrid nanofluids have not been used for enhancing mass transfer of wall jet under magnetic field. There is a lack of study on effects of physical terms, such as magnetic field, Brownian motion, thermal radiation, and thermophoresis, on temperature, momentum and entropy generation of ferro-hybrid nanofluids with heat and mass transfer.

With this motivation, the aim of the current numerical study is to examine the incompressible wall jet ferro-hybrid nanofluid movement and entropy generation in magnetic field. The authors noted that there is a dearth of study on wall jet fluid flows with the influence of volume fractions, magnetohydrodynamics, entropy analysis. To address the research gap, we will examine the influence of the Brinkman ratio, magnetic field, thermal radiation, thermophoresis, and Brownian motion on entropy generation with irreversible mechanism in wall jet ferro-hybrid nanofluid flows. This offers a wide-ranging method for grasping entropy creation in mass and energy transfer processes and improve the system thermal efficiency. Wall-jet ferro-hybrid nanofluid flow performs a major role in raising thermal transfer efficiency in advanced cooling systems. It is extensively utilized in industrial applications such as thermal management, energy systems, and microfluidic devices.

2. Mathematical analysis

Consider a hybrid fluid movement across an expanding sheet with energy and concentration T_p and C_p. Impact of radiation considered on hybrid nanofluid movement. The surfaces x_p and y_p are chosen along and normal to the sheet. The physical flow diagram is represented in Fig. 1. Governing equations of velocity, mass, and heat transfer with their boundaries are established to a set of ODEs through similarities.

A. **The following assumptions are discussed in this analysis:**

- Applied inclined magnetic field.
- Fluids are Newtonian.
- Chemical reaction is negligible.
- Pressure gradient is negligible i.e., $\nabla p = 0$.
- Flow is steady, laminar and incompressible i.e., $\frac{\partial u}{\partial t} = 0$.

2.1. Governing equations

Steady-state fluid flow assumptions two-dimensional nanofluid jets across the plane surface with the magnetic field as [6,10,27,28]

$$\frac{\partial u_p}{\partial x_p}+\frac{\partial v_p}{\partial y_p}=0, \tag{1}$$

$$u_p\frac{\partial u_p}{\partial x_p}+v_p\frac{\partial u_p}{\partial y_p}=\frac{\mu_{eff}}{\rho_{hnf}}\frac{\partial^2 u_p}{\partial y_p^2}-\frac{\sigma_{hnf}}{\rho_{hnf}}\mathrm{Sin}^2(\tau)B_0^2u_p, \tag{2}$$

$$\left(u_p\frac{\partial T_p}{\partial x_p}+v_p\frac{\partial T_p}{\partial y_p}\right)=\frac{\kappa_{hnf}}{(\rho Cp)_{hnf}}\frac{\partial^2 T_p}{\partial y_p^2}-\frac{1}{(\rho Cp)_{hnf}}\frac{\partial q_r}{\partial y}+\tau\left(D_B\frac{\partial C_p}{\partial y_p}\frac{\partial T_p}{\partial y_p}+\frac{D_T}{T_\infty}\left(\frac{\partial T_p}{\partial y_p}\right)^2\right) \tag{3}$$

$$u_p\frac{\partial C_p}{\partial x_p}+v_p\frac{\partial C_p}{\partial y_p}=D_B\frac{\partial^2 C_p}{\partial y_p^2}+\frac{D_T}{T_\infty}\frac{\partial^2 T_p}{\partial y_p^2}, \tag{4}$$

The boundary conditions are expressed as [6,63,64].

$$\begin{matrix} u_p=u_{wp}(x_p), & v_p=0, & T_p=T_{wp}, & C_p=C_{wp} & \text{at} & y_p=0,\\ u_p\to 0, & & T_p\to T_\infty, & C_p\to C_\infty & \text{as} & y_p\to\infty. \end{matrix} \tag{5}$$

where u_p and v_p are the component of velocity respectively, variable wall velocity defined as $u_{wp}(x_p)=\frac{Ud}{\sqrt{x_p/l_d}}$, where l_d is characteristic length, μ_{eff} is the effective viscosity, μ is the dynamic viscosity, ν is the dynamic viscosity, ρ denotes density, κ is the thermal conductivity, σ is the electrical conductivity, T_p is the temperature and C_p is concentration, q_r is the radiative heat flux, $B(x_q)=x_q^{-3/4}$, D_B is mass diffusion, D_T is the thermophoresis. Subscript, *hnf*, denotes hybrid nanofluid, and (τ) is the inclined angle.

The radiation flux is written using Rosseland estimation as [15–17]

$$q_r=-\frac{4\sigma^*}{3k^*}\frac{\partial T_p^4}{\partial y_p}, \tag{6}$$

Where σ* and k* are Stefan-Boltzmann and mean absorption terms.

$$T_p^4\cong 4T_\infty^3T_p-3T_\infty^4 \tag{7}$$

The radiation expression in Eq. (3) is calculated as.

$$\frac{\partial q_r}{\partial y}=-\frac{16\sigma^*T_\infty^3}{3k^*}\frac{\partial^2 T_p}{\partial y_p^2}, \tag{8}$$

2.2. Dimensionless governing equations

We can define the dimensionless variables as follows [63,64]:

$$x_q=\frac{x_p}{l_d},y_q=\frac{y_p}{l_d},u_q=\frac{u_p}{U_d},v_q=\frac{v_p}{U_d},Re_{l_d}=\frac{u_{wp}l_d}{\nu},$$

$$U_d=\frac{\nu}{l_d},T_q=\frac{T_p-T_\infty}{T_{wp}-T_\infty},C_q=\frac{C_p-C_\infty}{C_{wp}-C_\infty}, \tag{9}$$

Using the dimensionless variables, the governing Eqs. (1)–(4) are converted as follows:

$$\frac{\partial u_q}{\partial x_q}+\frac{\partial v_q}{\partial y_q}=0, \tag{10}$$

$$u_q\frac{\partial u_q}{\partial x_q}+v_q\frac{\partial u_q}{\partial y_q}=\frac{\Lambda}{A_2}\frac{\partial^2 u_q}{\partial y_q^2}-\frac{A_3}{A_2}\mathrm{Sin}^2(\tau)\frac{\sigma_f B_0^2B^2(x_q)l_d}{\rho_f U_d}u_q, \tag{11}$$

$$\left(u_q\frac{\partial T_q}{\partial x_q}+v_q\frac{\partial T_q}{\partial y_q}\right)=\frac{(A_4+Nr)}{A_5Pr}\frac{\partial^2 T_q}{\partial y_q^2}+Nb\frac{\partial C_q}{\partial y_q}\frac{\partial T_q}{\partial y_q}+Nt\left(\frac{\partial T_q}{\partial y_q}\right)^2, \tag{12}$$

$$u_q\frac{\partial C_q}{\partial x_q}+v_q\frac{\partial C_q}{\partial y_q}=\frac{1}{LePr}\left(\frac{\partial^2 C_q}{\partial y_q^2}+\frac{Nt}{Nb}\frac{\partial^2 T_q}{\partial y_q^2}\right) \tag{13}$$

Where $A_2=\frac{\rho_{hnf}}{\rho_f}$, $A_3=\frac{\sigma_{hnf}}{\sigma_f}$, $A_4=\frac{\kappa_{hnf}}{\kappa_f}$, $A_5=\frac{(\rho Cp)_{hnf}}{(\rho Cp)_f}$. $\Lambda\left(=\frac{\mu_{eff}}{\mu_f}\right)$ is the Brinkman/viscosity ratio parameter.

Similarity variables are defined as [63,64]:

$$\begin{matrix} \psi=x_q^{1/4}f(\eta), & u_q=x_q^{-1/2}f_\eta(\eta), & \eta=x_q^{-3/4}y_q,\\ v_q=-\frac{1}{4}x_q^{-3/4}(f(\eta)-3\eta f_\eta(\eta)), & T_q=\theta(\eta), & C_q=\varphi(\eta). \end{matrix} \tag{14}$$

By using similarity variables Eq. (14) the governing Eqs. (11)–(14) calculated as

$$\frac{\Lambda}{A_2}\frac{d^3f(\eta)}{d\eta^3}+\frac{1}{4}f(\eta)\frac{d^2f(\eta)}{d\eta^2}+\frac{1}{2}\left(\frac{df(\eta)}{d\eta}\right)^2-\frac{A_3}{A_2}M\mathrm{Sin}^2(\tau)\frac{df(\eta)}{d\eta}=0, \tag{15}$$

$$\frac{(A_4+Nr)}{A_5Pr}\frac{d^2\theta(\eta)}{d\eta^2}+\frac{1}{4}f(\eta)\frac{d\theta(\eta)}{d\eta}+Nb\frac{d\varphi(\eta)}{d\eta}\frac{d\theta(\eta)}{d\eta}+Nt\left(\frac{d\theta(\eta)}{d\eta}\right)^2=0, \tag{16}$$

$$\frac{d^2\varphi(\eta)}{d\eta^2}+\frac{1}{4}LePrf(\eta)\frac{d\varphi(\eta)}{d\eta}+\frac{Nt}{Nb}\left(\frac{d^2\theta(\eta)}{d\eta^2}\right)=0, \tag{17}$$

where

$Nt=\frac{\tau D_T\left(T_{wp}-T_\infty\right)}{\nu T_\infty}$, is the thermophoresis parameter,

$M=\frac{\sigma_f B_0^2 l_d}{aU_d}$ is a magnetic parameter,

$Pr=\frac{\nu_f}{\alpha_f}$ is the Prandtl number,

$Le=\frac{\alpha_f}{D_B}$ is the Lewis number,

$Nb=\frac{\tau D_B\left(C_{wp}-C_\infty\right)}{\nu}$, is the Brownian parameter,

$Nr=\frac{16\sigma^*T_\infty^3}{3k^*k_f}$, is the thermal radiation.

The boundary conditions are converted as [6,27,31,63]

$$\begin{matrix} f(0)=0, & f'(0)=d, & \theta(0)=1, & \varphi(0)=1, & \text{at} & \eta=0,\\ & f_\eta(\eta)=0, & & \theta(\eta)=0, & \varphi(\eta)=0, & \text{as} & \eta\to\infty. \end{matrix} \tag{18}$$

2.3. Analysis of entropy generation (Ng)

The *Ng* of the magnetic nanofluid is studied as [13–17].

Table 1
Thermophysical characteristics of base fluids and nanoparticles at 298.15 K, and under common circumstances see [35–37].

Properties	H_2O	Fe_3O_4	CuO
σ	5.5×10^{-6}	0.74×10^{6}	6.9×10^{-2}
ρ	997.1	5180	6500
Cp	4179	670	533
κ	0.6071	9.7	17.65

Table 2
Variation of $f''(0)$ for the various choices of M for $\phi_1, \phi_2, \Lambda = 0, \tau = 90^{\circ}$.

M	Akbar et al. [24]	Abdelmalek [25]	Fatehzadeh et al. [26]	Present results
0	−1	−1.004	−1	−1.0281
0.5	−1.11803	−1.1180	–	−1.1180
1.0	−1.41421	−1.4140	1.41412	−1.4140
5.0	−2.44949	−2.4494	−2.44948	−2.4498
10	−3.31663	−3.3168	−3.31662	−3.3191

$$Sg=\frac{\kappa_{hnf}}{T_\infty^2}\left[A_4+\frac{16\sigma^*T_\infty^3}{3k^*\kappa_f}\right]\left(\frac{\partial T_q}{\partial y_q}\right)^2+Nb\left(\frac{\partial C_q}{\partial y_q}\frac{\partial T_q}{\partial y_q}\right)+Nt\left(\frac{\partial T_q}{\partial y_q}\right)^2, \tag{19}$$

$$\text{Energy loss via heat transfer}\Rightarrow\frac{\kappa_{hnf}}{T_\infty^2}\left[A_4+\frac{16\sigma^*T_\infty^3}{3k^*\kappa_f}\right]\left(\frac{\partial T_q}{\partial y_q}\right)^2, \tag{20}$$

The entropy production rate is calculated as

$$Ng=\frac{\nu_f T_\infty}{(U_d/l_d)\kappa_f(T_{wp}-T_\infty)}Sg$$
$$=(A_4+Nr)\delta\left(\frac{d\theta(\eta)}{d\eta}\right)^2+Nb\frac{d\theta(\eta)}{d\eta}\frac{d\varphi(\eta)}{d\eta}+Nt\left(\frac{d\theta(\eta)}{d\eta}\right)^2 \tag{21}$$

where temperature difference parameter $\delta=\frac{T_{wp}-T_\infty}{T_\infty}$.

2.4. Calculation of engineering quantities [6,32,63]

The skin friction, C_f, Nusselt number and Sherwood numbers are calculated as

$$C_f=\frac{1}{\rho u_{wp}^2(x_p)}\left(\left(\mu_{eff}\right)\frac{\partial u_p}{\partial y_p}\bigg|_{y_p=0}\right) \tag{22}$$

$$Nu_{x_p}=\frac{x_p}{\kappa_f(T_{wp}-T_\infty)}\left(-\left(\kappa_{hnf}+\frac{16\sigma^*T_\infty^3}{3k^*}\right)\left(\frac{\partial T_p}{\partial y_p}\right)\bigg|_{y_p=0}\right), \tag{23}$$

$$Sh_{x_p}=\frac{x_p}{D_f(C_{wp}-C_\infty)}\left(-D_f\left(\frac{\partial C_p}{\partial y_p}\right)\bigg|_{y_p=0}\right), \tag{24}$$

the above Eqs. (22)–(24) transformed by using Eq. (9) as follows

$$C_f=\frac{1}{u_{wq}^2(x_q)}\left(\left(\frac{\mu_{eff}}{\mu_f}\right)\frac{\partial u_q}{\partial y_q}\bigg|_{y_q=0}\right) \tag{25}$$

Table 3
Variation of $-\theta'(0)$ for the various choices of Pr, Nt, Nb for $\phi_1, \phi_2, Nr = 0$.

Pr	Nb	Nt	Abdelmalek [25]	Present results
2.0	0.1	0.1	0.7406	0.76611
5.0			0.9060	0.91289
7.0			1.1717	1.19980
10.0			1.4522	1.41125
2.0	0.1		0.7406	0.71156
	0.2		0.6415	0.64557
	0.3		0.5538	0.52561
	0.5		0.4089	0.40011
	0.1	0.1	0.7406	0.73332
		0.2	0.6840	0.67992
		0.3	0.6328	0.63299
		0.4	0.5866	0.58134

Table 4
Variation of $-\varphi'(0)$ for the various choices of Pr, Nt, Nb, Le for $\phi_1, \phi_2, Nr = 0$.

Pr	Nb	Nt	Le	Abdelmalek [25]	Present work
2.0	0.1	0.1	3.0	1.4724	1.52334
5.0				2.7225	2.88111
7.0				3.1488	3.14141
10.0				4.3319	4.42211
2.0	0.1			1.4724	1.37667
	0.2			1.6489	1.66132
	0.3			1.7044	1.70331
	0.5			1.7435	1.73445
	0.1	0.1		1.4724	1.47474
		0.2		1.2678	1.26788
		0.3		1.1228	1.28898
		0.4		1.0258	1.02580
		0.1	3.0	1.4724	1.47240
			5.0	2.1085	2.20201

$$Nu_{x_p}=\left(-\left(\frac{\kappa_{hnf}}{\kappa_f}+\frac{16\sigma^*T_\infty^3}{3k^*\kappa_f}\right)x_q\left(\frac{\partial T_q}{\partial y_q}\right)\bigg|_{y_q=0}\right), \tag{26}$$

$$Sh_{x_p}=\left(-x_q\left(\frac{\partial C_q}{\partial y_q}\right)\bigg|_{y_q=0}\right), \tag{27}$$

further Eqs. (25)–(27) calculated by utilizing Eq. (14) as follows

$$\mathrm{Re}_{l_d}^{1/2}C_f=\Lambda f''(0), \tag{28}$$

$$\mathrm{Re}_{l_d}^{-1/2}Nu_{x_q}=-(A_4+Nr)\theta'(0), \tag{29}$$

$$\mathrm{Re}_{l_d}^{-1/2}Sh_{x_q}=-\varphi'(0), \tag{30}$$

$\mathrm{Re}_{l_d}=\frac{u_{wq}l_d}{\nu_f}$ is the Reynolds number,

3. Numerical approach with solution

The Numerical approach allows you to evaluate nonlinear governing formulations using partial derivatives. This procedure delivers more exact conclusions than previous numerical approaches.

In order to transform more order into a linear differential equation, we are adding new terms.

$$y_1=f,\ y_2=f',\ y_3=f'',\ y_4=\theta,\ y_5=\theta',\ y_6=\varphi,\ y_7=\varphi'. \tag{31}$$

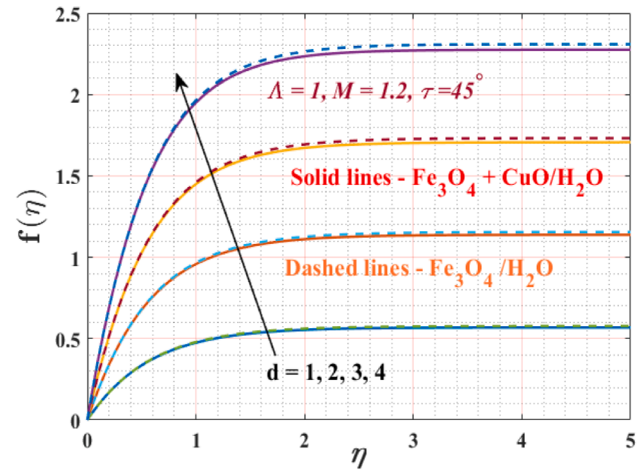

(a) transverse velocity

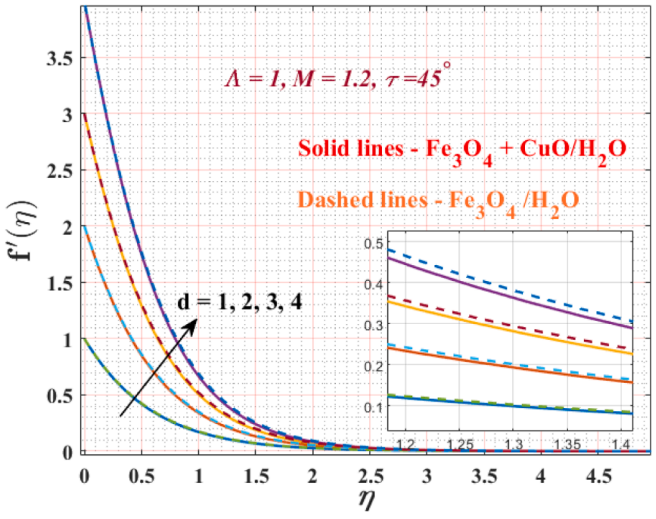

(b) axial velocity

Fig. 2. Effects of stretching parameter (d) on velocities: (a) Transverse, and (b) axial velocity.

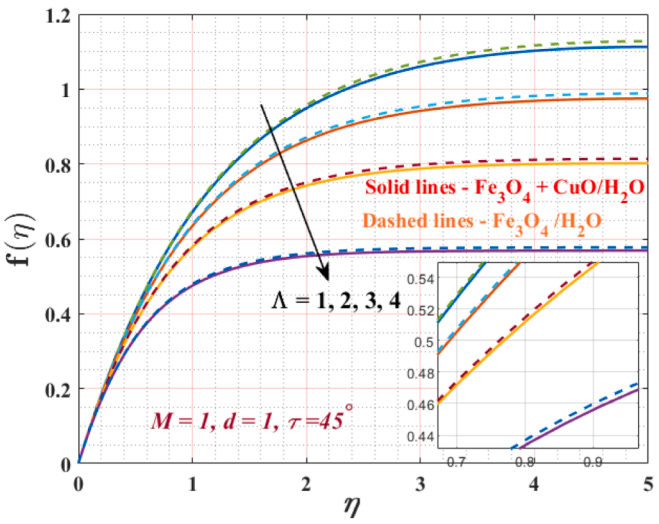

(a) transverse velocity

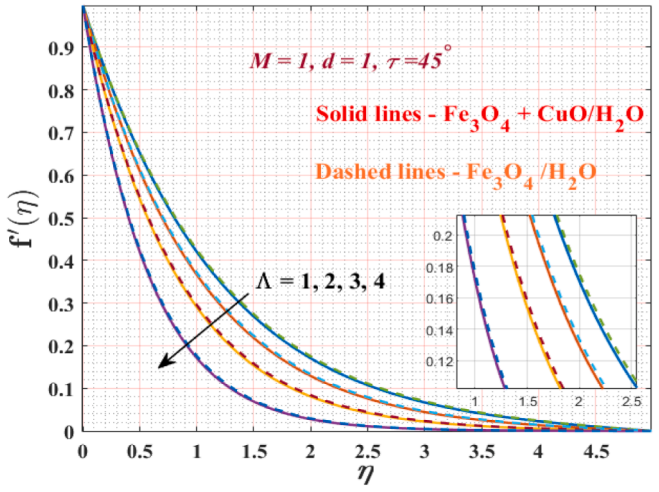

(b) axial velocity

Fig. 3. Effects of Brinkman number (**Λ**) on velocities: (a) Transverse and axial velocity.

The governing Eqs. (15)–(17) are calculated as

$$y_2^1 = y_3,\ y_3^1 = \left(\left(\frac{A_2}{\Lambda}\right)\left(-\frac{1}{4}y_1y_2 - \frac{1}{2}y_2^2 + \frac{A_3}{A_2}M\mathrm{Sin}^2(\tau)y_2\right)\right),$$
$$y_4^1 = y_5,\ y_5^1 = \left(\left(\frac{A_5Pr}{(A_4+Nr)}\right)\left(-\frac{1}{4}y_1y_5 - Nby_5y_7 - Nty_5^2\right)\right), \tag{32}$$
$$y_6^1 = y_7,\ y_7' = \left(-\frac{1}{4}LePry_1y_7 - \frac{Nt}{Nb}\left(\left(\frac{A_5Pr}{(A_4+Nr)}\right)\left(-\frac{1}{4}y_1y_5 - Nby_5y_7 - Nty_5^2\right)\right)\right),$$

3.1. The model verification

To verify the model, we test the model using the properties of nanoparticles in Table 1 and data available [24–26]. Table 2 shows a comparison of $f''(0)$ between our modelled results and those by Akbar et al. [24], Abdelmalek [25] and Fatehzadeh et al. [26] at $\phi_1, \phi_2, \Lambda = 0,\ \tau = 90^\circ$. Our results are in agreement with their ones with less than 1 % errors. It can be found that $-\theta'(0)$ using our model agrees well with that by Abdelmalek [25] in terms of various Pr, Nt, Nb when $\phi 1, \phi 2, Nr = 0$ (Table 3). To verify our model further, we perform a comparison of $-\varphi'(0)$ with data by Abdelmalek [25] (Table 4). It can be found that the present model agrees well with data by Abdelmalek [25].

$$\left.\begin{aligned}
\frac{\rho_{hnf}}{\rho_f} &= (1-\phi_2)\left(1-\phi_1+\phi_1\left(\frac{\rho_{s_1}}{\rho_f}\right)\right)+\phi_2\left(\frac{\rho_{s_2}}{\rho_f}\right),\\
\frac{\sigma_{hnf}}{\sigma_f} &= \frac{\sigma_{s_2}+2\sigma_{bf}+2\phi_2(\sigma_{s_2}-\sigma_f)}{\sigma_{s_2}+2\sigma_{bf}-\phi_2(\sigma_{s_2}-\sigma_f)},\\
&\text{where}\\
\frac{\sigma_{bf}}{\sigma_f} &= \frac{\sigma_{s_1}+2\sigma_f+2\phi_1(\sigma_{s_1}-\sigma_f)}{\sigma_{s_1}+2\sigma_f-\phi_1(\sigma_{s_1}-\sigma_f)}\\
\frac{\mu_{hnf}}{\mu_f} &= \frac{1}{(1-\phi_1)^{2.5}(1-\phi_2)^{2.5}},\\
\frac{(\rho C_p)_{hnf}}{(\rho C_p)_f} &= (1-\phi_2)\left(1-\phi_1+\phi_1\left(\frac{(\rho C_P)_{s_1}}{((\rho C_P)_f}\right)\right)+\phi_2\left(\frac{((\rho C_P)_{s_2}}{(\rho C_P)_f}\right)\\
\frac{\kappa_{hnf}}{\kappa_f} &= \frac{\kappa_{s_2}+2\kappa_{bf}+2\phi_2(\kappa_{s_2}-\kappa_f)}{\kappa_{s_2}+2\kappa_{bf}-\phi_2(\kappa_{s_2}-\kappa_f)},\\
&\text{where}\\
\frac{\kappa_{bf}}{\kappa_f} &= \frac{\kappa_{s_1}+2\kappa_f+2\phi_1(\kappa_{s_1}-\kappa_f)}{\kappa_{s_1}+2\kappa_f-\phi_1(\kappa_{s_1}-\kappa_f)},
\end{aligned}\right\} \quad (29)$$

where S_1 and S_2 represent Fe_3O_4 and CuO nanoparticles [6,34,35].

4. Results and discussion

The current study explores the influence of the Brinkman ratio and variable magnetic field on wall jet ferro hybrid nanofluid (HNF) with energy and mass transfer with entropy generation analysis. HNF materials are formed by mixing ferrous-ferric oxide (Fe_3O_4) and Copper oxide (CuO) in conventional fluid water. Applying these tiny particles to the water will enrich heat transfer. Several parameters are explained through graphs in this section. In all the below figures, solid lines represent the hybrid nanofluid flows oxide ($Fe_3O_4 + CuO$) and dash lines do the single nanofluid (Fe_3O_4). Bottom corner figures are locally the zoomed-in figure.

4.1. Influence of physical terms on the momentum of the fluid flow

Here we considered the stretching term, Brinkman ratio, and magnetic field impact on the transverse and axial velocity of the fluid. Fig. 2 (a) and (b) portrays the transverse and axial velocity under various choices of stretching parameters. As the stretching term (d) raises, both the transverse and axial momentum increase for the hybrid and nanofluid movements. Thus, rising the d term rises the momentum of the fluid movement. However, it can be seen that the increases of main transverse and axial velocity are different. While the transverse velocity increases are at $\eta > 0.5$, the axial velocity increases are at $\eta < 1.5$. For example, the transverse velocity increases to 4 at $d = 4$ from 1 at $d = 1$ when $\eta = 0$ but it has no changes when $\eta = 5$. In contrast, the axial velocity increases to 2.25 at $d = 4$ from 0.51 at $d = 1$ when $\eta = 0$ but it has no changes when $\eta = 5$. This shows that the effects of d on velocities are heterogeneous in the domain. Physically, raise in the stretching term enhances the axial momentum as the momentum upsurges, leading to a higher velocity profile along the stretching sheet. However, the hybrid nanofluids slightly increase the transverse velocity, compared to the single nanofluid while axial velocities are similar clearly see that in bottom corner zoomed graph in Fig. 2b.

Fig. 3 shows effects of Brinkman number ($\mathbf{\Lambda}$) on transverse and axial velocity when $M = 1, d = 1, \tau = 45^{\circ}$. Solid lines represent the hybrid nanofluid flows oxide ($Fe_3O_4 + CuO$) and dash lines do the single nanofluid (Fe_3O_4). It can be found that as the Brinkman number increases the transverse and axial velocities decrease. Furthermore, the transverse velocities increase at a fixed $\mathbf{\Lambda}$ as η increases. Brinkman number ($\mathbf{\Lambda}$) has not affected the transverse velocities at $\eta = 0$ but has significantly influences when $\eta > 1.5$. However, the axial velocities decrease at a fixed $\mathbf{\Lambda}$ as η increases. Brinkman number ($\mathbf{\Lambda}$) has significant effects on the axial velocities at $\eta = 1.25$ but decreases effects as η increases or decreases. Physically, the momentum profile decays with increasing the Brinkman number. This difference between transverse and axial velocities results from slip condition occurring while the momentum of the expanding surface is not the same as the momentum near the surface. It can be found that the hybrid nanofluids slightly decrease the transverse and axial velocities, compared to the single nanofluid in the bottom corner zoomed graph in Fig. 3.

Fig. 4(a) and (b) represent the transverse and axial velocity plots for various choices of magnetic parameters, here plots are taken for hybrid and nanofluid movements, enhancing the magnetic term decays the momentum of the fluid. Bottom corner figures are the zoomed graphs of Fig. 4(a) and (b) in that zoomed plots we can clearly see the difference of nanofluid and hybrid nanofluid effects for magnetic field. Physically, the inclusion of a magnetic effect produces a Lorentz force that opposes the fluid motion, outcomes in a reduction of momentum, especially near the boundary layer. This effect is pronounced in electrically conducting fluids, where the magnetic field can suppress velocity fluctuations and create deceleration zones.

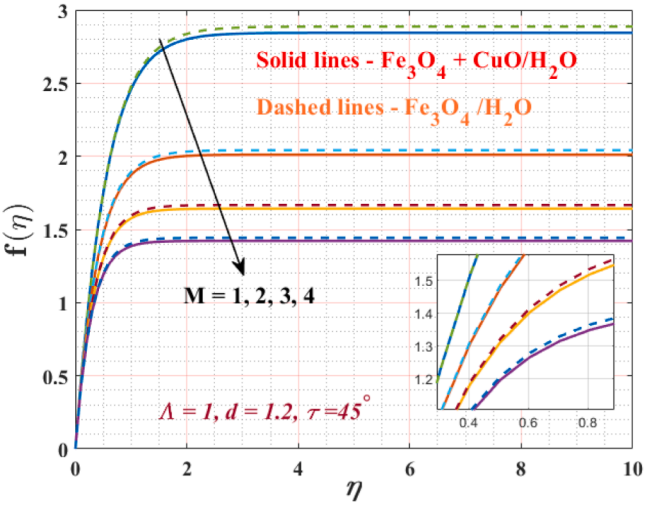

(a) transverse velocity

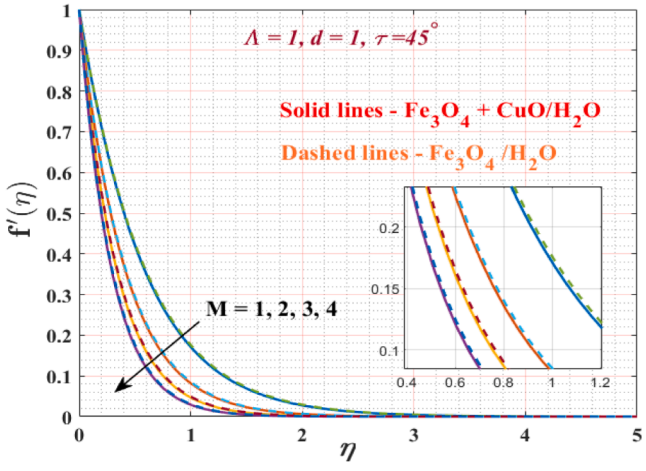

(b) axial velocity

Fig. 4. Effects of magnetic term (M) on velocities: (a) Transverse, and (b) axial velocity.

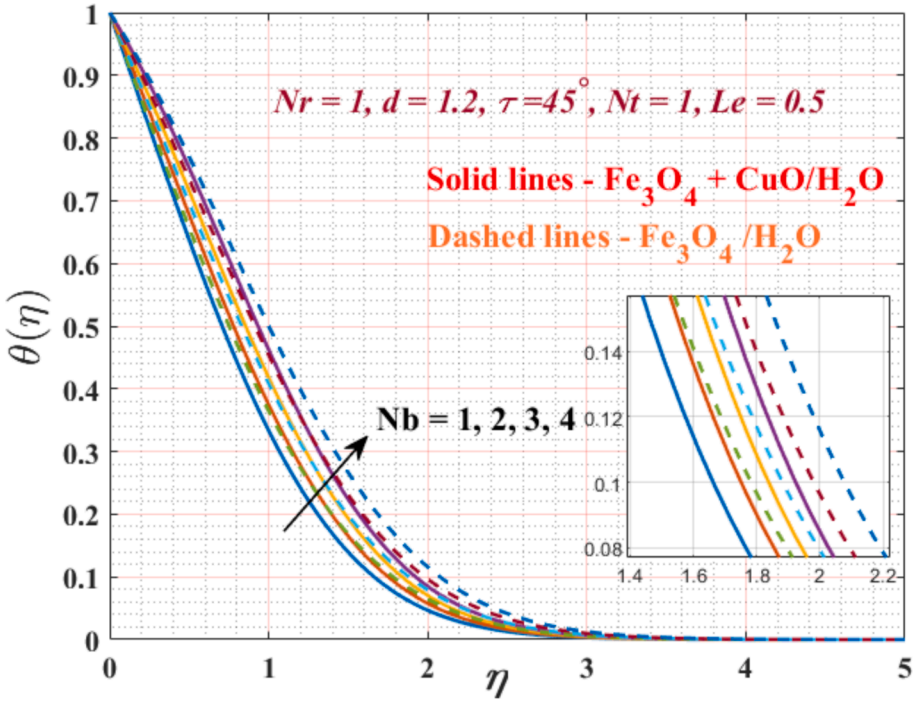

Fig. 5. Brownian movement impact on temperature.

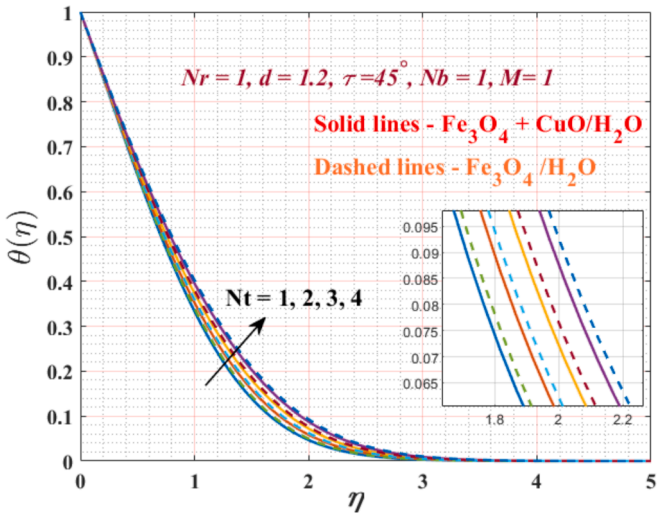

Fig. 6. Impact of thermophoretic parameter (*Nt*) on temperature.

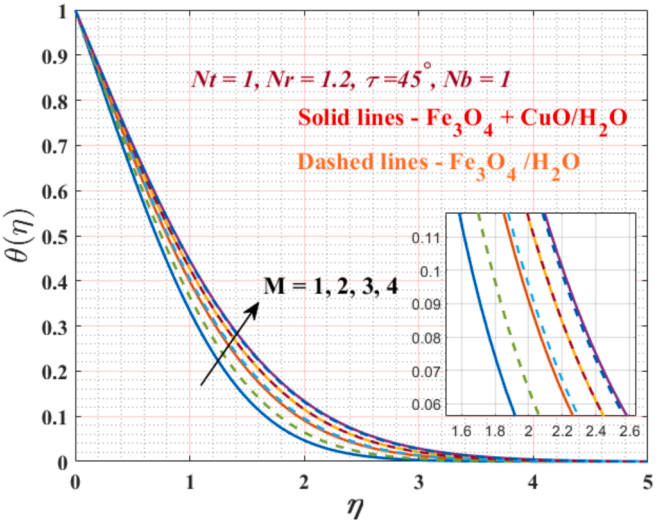

Fig. 7. Impact of magnetic term (*M*) on temperature.

4.2. *Influences of physical terms on the temperature of the fluid flow*

Here we considered impact of thermophoresis, Brownian motion, radiation, and magnetic field on the energy of the fluid. Fig. 5 portrays impact of the Brownian parameters on the temperature when other parameters are fixed. It can be found that the energy profile raises as the Brownian term increases, particularly in the middle range of η. Furthermore, the hybrid nanofluids have more effects on the temperature than the single nanofluid flows as shown in the zoomed-in part of Fig. 5. Physically, an increasing the Brownian movement parameter represents an increase in the nanofluid particle movement within the liquid, leading to an increasing heat transfer and temperature profile in the temperature. Because of higher heat transfer, the hybrid nanofluids lead to higher temperatures, compared to the single nanofluid.

Fig. 6 shows impact of *Nt* term on temperature. It can be found that upsurging the *Nt* parameter increases the fluid temperature. Bottom corner zoomed-in graph of Fig. 6 shows that effects of thermophoretic parameter on temperature for the hybrid nanofluids are greater than that for the single nanofluid. zoomed graph we can clearly see the difference of nanofluid and hybrid nanofluid effects for thermophoretic parameter. Physically, rise in the *Nt* term tends to raises the temperature. This is due to enhanced thermal gradients that facilitate better heat transfer within the fluid. Enhances in the choices of the *Nt* parameter accelerate the energy and mass transfer rates. The hybrid nanofluids lead to higher heat transfer due to their higher thermal conductivity than the single nanofluid.

Fig. 7 demonstrates effects of magnetic term (*M*) on energy. It can be found that the temperature rises as the *M* term raises. However, there is a difference for impact of magnetic field on single nanofluid and hybrid nanofluid as shown in the bottom corner zoomed-in graph of Fig. 7.

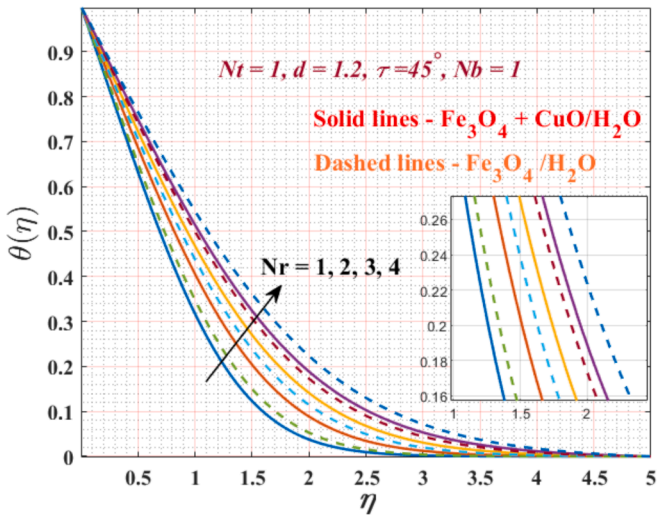

Fig. 8. *Nr* effect on temperature.

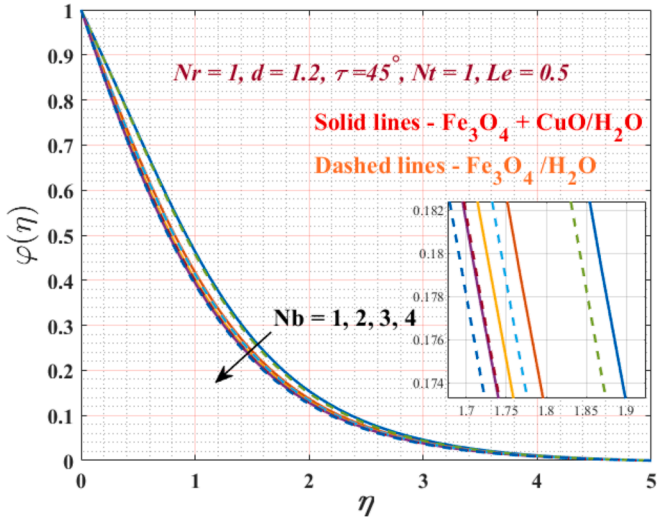

Fig. 9. Impact of *Nb* on concentration.

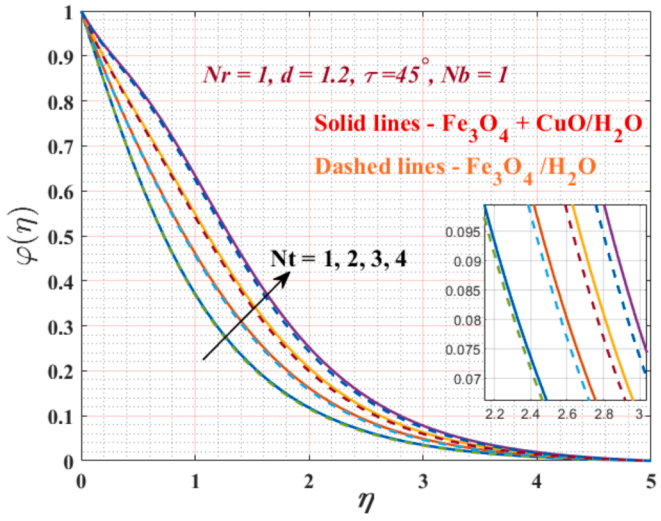

Fig. 10. Graph of thermophoretic parameter on concentration.

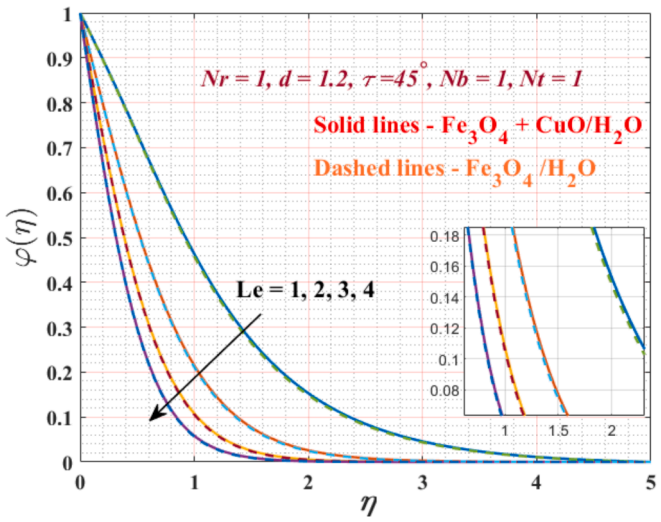

Fig. 11. Influence of Lewis number parameter on concentration.

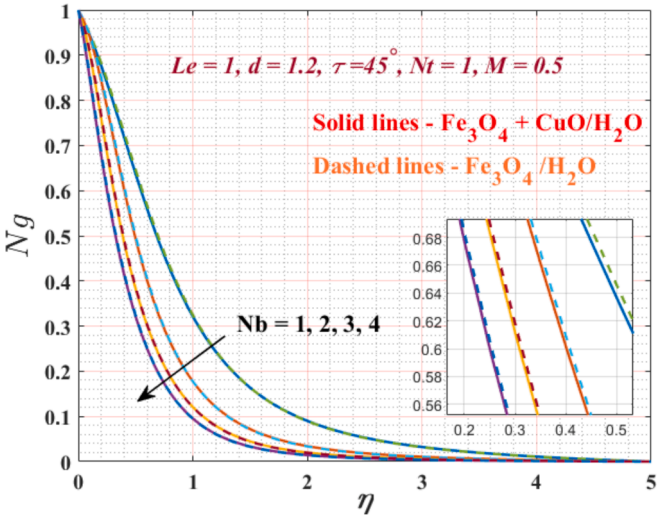

Fig. 12. Effects of Brownian motion (*Nb)* on *Ng*.

When the magnetic term is 1, the temperature of the hybrid nanofluids increases greater than that of single nanofluid. However, as the magnetic parameter increases, its effects on nanofluid and hybrid nanofluids decreases. After $M = 3$, the difference between them can be neglected. This is due to Lorentz force obtained by the magnetic effect, which reduces the fluid movement and can reduce convective heat transfer rates.

Fig. 8 shows influence of thermal radiation term (*Nr*) on temperature. It can be found that the energy increases as *Nr* raises. However, the energy of the hybrid nanofluid increases above than that of the nanofluid as *Nr* increases. This is because thermal radiation values provide more energy to the working fluid, resulting in enhanced energy and thermal boundary thickness. Thus, higher thermal conductivity of the hybrid nanofluid increases greater temperature than that of single nanofluid.

4.3. *Effects of physical parameters on the concentration*

Here we considered the Lewis number, Brownian motion, and - thermophoresis effects on the temperature of the fluid movement.

Fig. 9 represents the energy and concentration plots for different choices of Brownian motion parameters, here graphs are taken for hybrid and nanofluid flows, rising the *Nb* decreases the concentration of

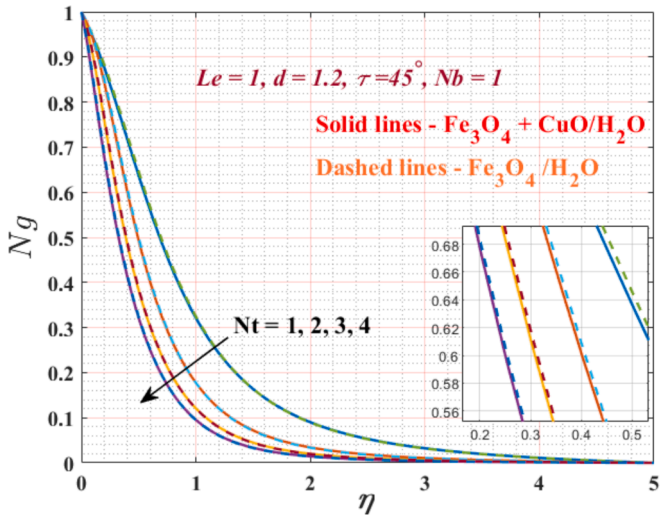

Fig. 13. Impact of the thermophoretic term (*Nt*) on the entropy generation (*Ng*).

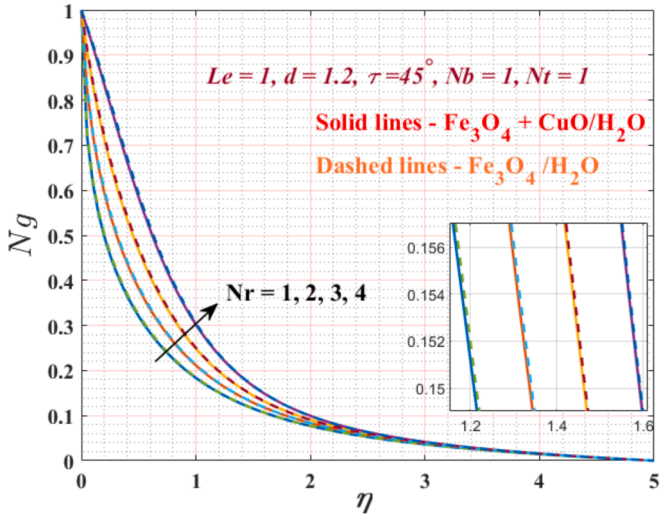

Fig. 14. Effects of the radiation term (*Nr*) on entropy generation.

the fluid movement. Bottom corner figure was the zoomed graph of Fig. 9 in that zoomed graph we can clearly see the difference of nanofluid and hybrid nanofluid effects for Brownian motion. Physically, enhancing the *Nb* term generally tends to a decay in nanoparticle concentration profiles. This effect is due to enhanced dispersion caused by the random motion of particles, which dilutes their concentration in the fluid. The average entropy generation tends to reduce as the *Nb* parameter upsurges. This is due to enhanced thermal energy transfer and dispersion of nanoparticles, which contributes to greater irreversibility in the system.

Fig. 10 portrays the concentration graphs for various choices of thermophoretic parameters, here graphs are taken for hybrid and nanofluid movements, rising the *Nt* term raises the concentration of the fluid. Bottom corner figure was the zoomed graph of Fig. 10 in that zoomed graph we can clearly see the difference of nanofluid and hybrid nanofluid effects thermophoretic parameter. Physically, higher thermophoretic values lead to enhanced dispersion of nanoparticles, resulting in higher concentrations in the fluid. Higher thermophoretic parameters lead to the decay of the entropy generation due to enhanced thermal gradients and particle movement. This results in greater irreversibility in the system.

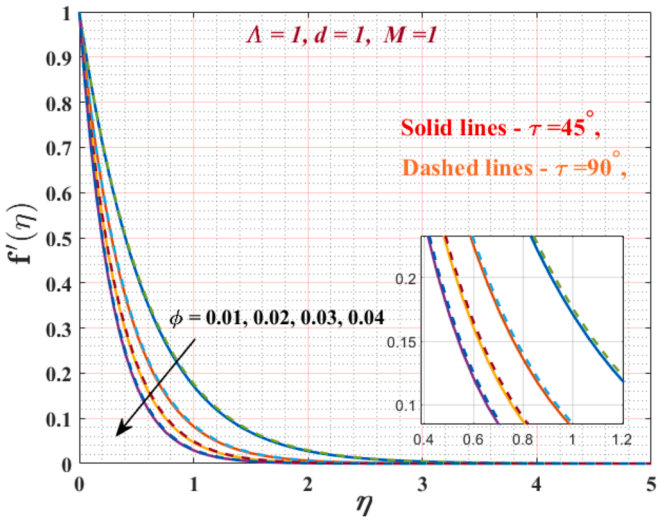

Fig. 15a. Volume fraction effect on axial velocity.

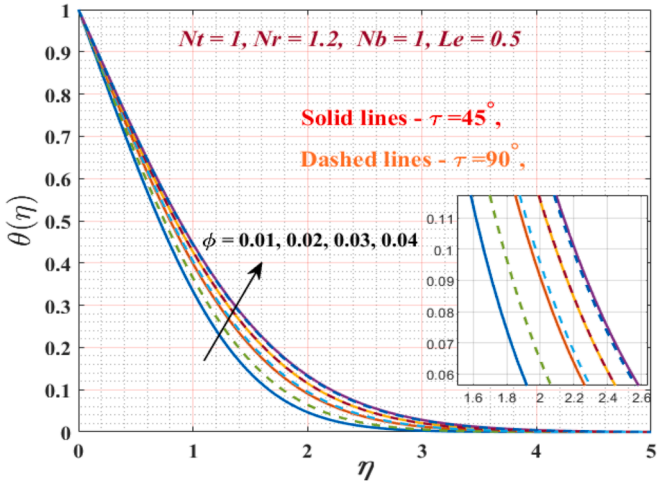

Fig. 15b. Volume fraction effect on temperature.

Fig. 11 portrays the concentration graph for various values of the *Le* term, here graphs are taken for hybrid and nanofluid flows, and rising the *Le* term reduces the concentration of the fluid movement. Bottom corner figure was the zoomed graph of Fig. 11 in that zoomed graph we can clearly see the difference of nanofluid and hybrid nanofluid effects for Lewis number. Upsurging the *Le* leads to a decay in the concentration of the diffusing species. This is due to momentum diffusivity and mass diffusivity ratio, which influences how quickly particles spread through the fluid.

4.4. Impact of physical terms on the entropy generation of the fluid flow

Here we considered the thermophoresis, Brownian motion, and radiation effects on the entropy generation of the fluid flow. Fig. 12 portrays effects of Brownian motion *Nb* on the entropy generation (Ng). It can be found that the *Ng* dreduces as Brownian motion increases. This is because increasing the *Nb* enhances thermal energy transfer and dispersion caused by the random motion of particles, which dilutes their concentration in the fluid and contributes to greater irreversibility in the system. Furthermore, there is a small difference between single nanofluid and hybrid nanofluid.

Fig. 13 portrays the impact of the *Nt* on the *Ng*. The entropy generation reduces as the thermophoretic parameters increase. This because

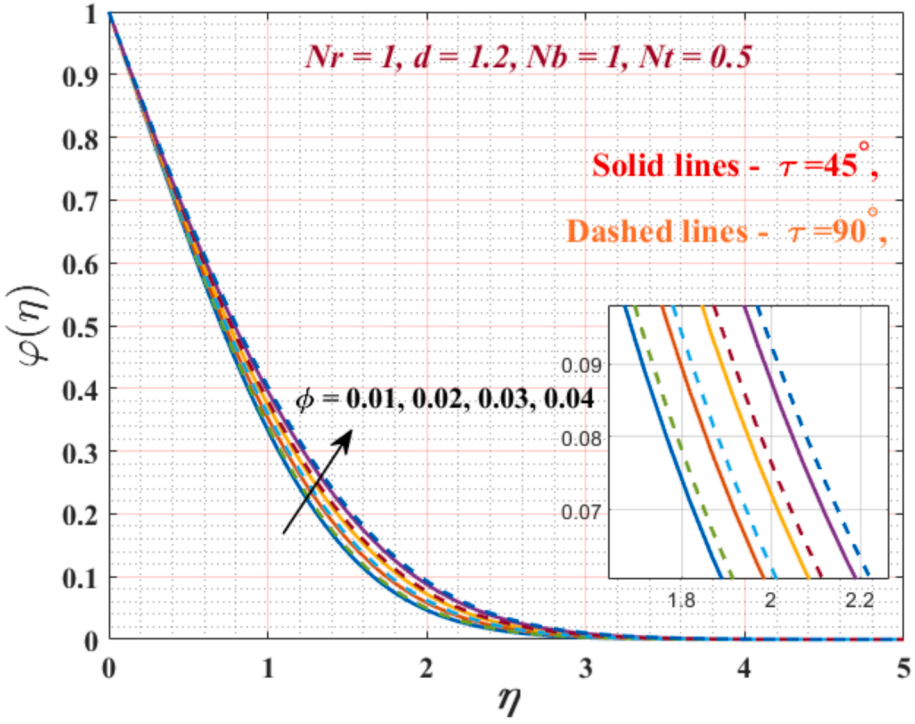

Fig. 16a. Volume fraction effect on concentration.

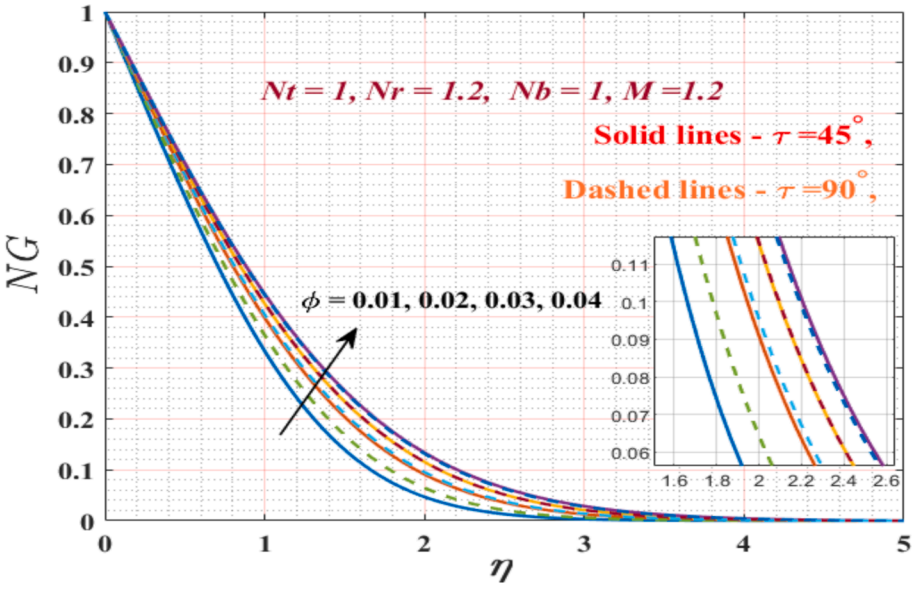

Fig. 16b. Volume fraction effect on entropy generation.

higher thermophoretic parameters lead to enhanced thermal gradients and particle movement. However, this results in greater irreversibility in the system. Furthermore, there is only a small difference of thermophoretic parameter effects between single nanofluid and hybrid nanofluid.

Fig. 14 represents impact of the thermal radiation term on the *Ng*. As *Nr* parameter increases entropy generation increases. This can be explained that higher thermal radiations provide more energy to the working fluid, resulting in enhanced temperature gradients and irreversibility in the system. However, there is no difference of thermal radiations on single nanofluid and hybrid nanofluid.

4.5. Impact of volume fraction on velocity, temperature, concentration and entropy generation of the fluid flow

Fig. 15(a) and (b) portrays the ϕ plots for axial momentum and temperature of the flow, raising the volume fraction decays the velocity and rising the energy of the fluid movement. Fig. 16(a) and (b) portrays the ϕ plots for concentration and entropy generation analysis, rising the volume fraction enhances the concentration as well as entropy generation analysis, Physically, the volume fraction of nanoparticles in a nanofluid significantly impacts entropy generation, which is influenced by thermal and fluid friction effects. As the volume fraction increases, thermal conductivity improves, reducing temperature gradients and

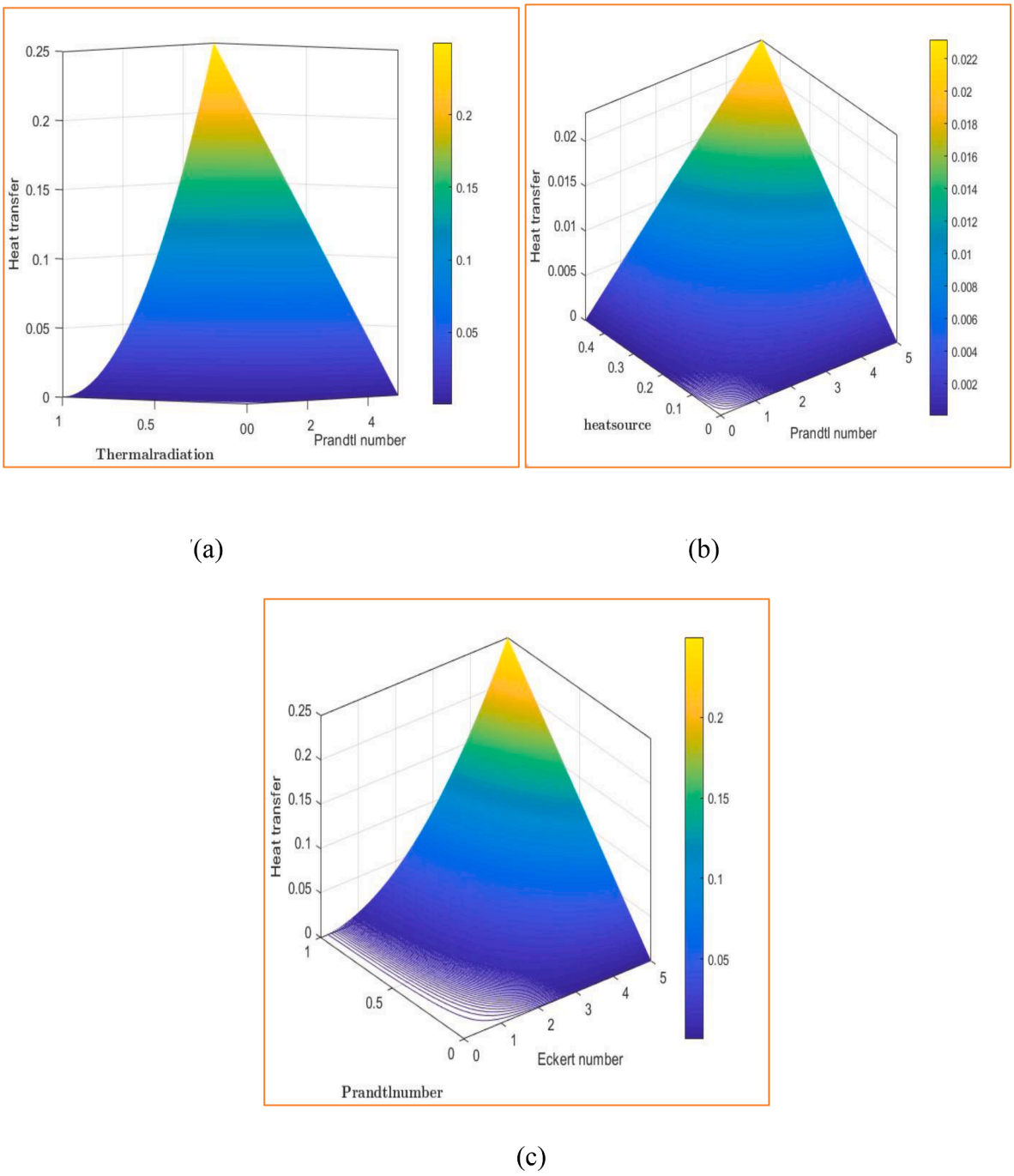

Fig. 17. (a), (b) and (c) represents the contour plot graphs for heat transfer.

entropy generation due to heat transfer. However, a higher volume fraction also increases viscosity, leading to greater fluid friction and higher entropy generation due to flow resistance. The overall impact on entropy generation depends on finding an optimal volume fraction where the reduction in thermal entropy outweighs the increase in frictional entropy. Proper balance ensures efficient energy utilization while minimizing irreversibility's.

4.6. *Contour plot graphs for temperature analysis*

Here we considered heat source, thermal radiation and Prandtl number impact on heat transfer plots the fluid movement (Fig. 17). Fig. 17(a), and (b) (c) visually represents the contour plot graphs for the heat transfer and spatial variation of these properties across a given system. In Fig. 17(a) shows impact of *Nr* and *Pr* on the heat transfer. It can be found that the heat transfer increases as both *Nr* and *Pr* increase. The highest transfer is in top areas while the lowest is in bottom. For thermal radiation, they highlight regions with varying radiative heat

flux. Fig. 17(b) and (c) show effects of heat source and *Ec* with Prandtl number on the heat transfer, respectively. The high heat transfer areas are found when both high heat source and Prandtl number. Similarly, the high heat transfer areas are when both high Eckert number and Prandtl number. The Prandtl number contours reflect the connection between momentum and thermal diffusivity, providing insights into fluid movement and thermal boundary layer behavior in the system.

5. Conclusion

Wall jet ferro hybrid nanofluid with mass and energy transfer has a numerous of applications, such as solar-based heat exchange, cooling electronics, energy storage, heat exchangers, and pharmaceuticals, due to their high heat and mass transfer. In this study, we explore the impact of the Brinkman ratio, Brownian motion, the thermal radiation, the thermophoretic parameters, and magnetic field on wall jet ferro single and hybrid nanofluid with mass and energy. with generation analysis. Hybrid nanofluid materials are formed by hybrid nanofluids of ferrous-ferric oxide and Copper oxide in water to enhance thermal and mass transfer. Partial differential governing equations of velocity, mass, and energy transfer with their boundary conditions are calculated to a set of ODEs using a set of similarity parameters. The ODEs are calculated using the Runge-Kutta method. The numerical results show that rising the magnetic field or Brinkman number decays the axial and transverse velocities. However, there are no velocity differences between single nanofluid and hybrid nanofluid. It is showed that rising the Brownian motion, the magnetic term, or the thermophoresis term raises the fluid temperature. Furthermore, Brownian movement, or the thermophoresis term increases energy more for the hybrid nanofluids than that for single nanofluid. However, effects of the magnetic term on the temperature of the hybrid nanofluids increases more than that of single nanofluid when the magnetic parameter is 1. After $M = 3$, the difference between them can be neglected. Increasing the thermophoretic parameters and Brown motion lead to the decay of the entropy generation due to enhanced thermal gradients and particle movement. However, the entropy generation raises as the radiation parameter raises. This demonstrates that the hybrid nanofluids can raise the heat and mass transfer but no impact on velocities and entropy generation, compared to the single nanofluid.

The results of the current study can be applied to increase the efficiency of electronic cooling systems by improving heat dissipation in compact devices. In solar collectors, optimizing ferrofluid flow can boost thermal energy absorption and conversion efficiency. Medical cooling devices, such as those used for localized therapeutic cooling, can benefit from precise temperature control enabled by improved heat and mass transfer. Additionally, the integration of magnetohydrodynamics allows for better flow manipulation in advanced thermal management systems.

The limitations of present analysis include challenges in accurately modeling the complex interactions between magnetic fields, nanoparticles, and fluid flow at high temperatures. Additionally, the stability of ferrofluids over time can be affected by particle aggregation and sedimentation, limiting long-term performance. The current work can be extended by including the impacts of Darcy-Forchheimer media, Joule heating, Newton heating effects over various boundaries such as wedge, convergent/divergent channel, exponential stretching sheet, Riga surface among others.

6. Code availability

Codes that support the findings of this study are available from the corresponding author upon reasonable request.

CRediT authorship contribution statement

S.M. Sachhin: Writing – review & editing, Writing – original draft, Visualization, Validation, Methodology, Investigation, Formal analysis, Data curation, Conceptualization. **U.S. Mahabaleshwar:** Writing – review & editing, Writing – original draft, Supervision, Software, Resources, Project administration, Formal analysis, Data curation, Conceptualization. **N. Swaminathan:** Writing – review & editing, Formal analysis, Conceptualization. **L.M. Pérez:** Writing – review & editing, Formal analysis, Data curation. **Junye Wang:** Writing – review & editing, Writing – original draft, Supervision, Formal analysis.

Declaration of competing interest

The authors declare that they have no known competing financial interests or personal relationships that could have appeared to influence the work reported in this paper.

Acknowledgement

LMP acknowledges financial support from ANID through *Convocatoria Nacional Subvención a Instalación en la Academia Convocatoria año 2021*, Grant number SA77210040 and FONDECYT 1240985.

Data availability

Data that support the findings of this study are available from the corresponding author upon reasonable request.

References

[1] E.H. Aly, U.S. Mahabaleshwar, T. Anusha, W.K. Usafzai, I. Pop, Wall jet flow and heat transfer of a hybrid nanofluid subject to suction/injection with thermal radiation, Therm. Sci. Eng. Prog. 32 (2022) 101294.
[2] W.K. Usafzai, A.M. Saeed, E.H. Aly, V. Puneeth, I. Pop, Wall jet nanofluid flow with thermal energy and radiation in the presence of power-law, Numer. Heat Transf. A Appl. 85 (14) (2024) 2367–2379.
[3] S.M. Sachhin, U.S. Mahabaleshwar, A. Chan, Effect of slip and thermal gradient on micropolar nano suspension flow across a moving hydrogen fuel-cell membrane, *Int. J. Hydrogen Energy* 63 (Apr. 2024) 59–81, https://doi.org/10.1016/j.ijhydene.2024.02.332.
[4] W. Khan Usafzai, R.U. Haq, E.H. Aly, Wall laminar nanofluid jet flow and heat transfer, Int. J. Numer. Meth. Heat Fluid Flow 33 (5) (2023) 1818–1836.
[5] S. Idris, A. Jamaludin, R. Nazar, I. Pop, Heat transfer characteristics of magnetized hybrid ferrofluid flow over a permeable moving surface with viscous dissipation effect, Heliyon 9 (5) (2023).
[6] S.M. Sachhin, U.S. Mahabaleshwar, D. Zeidan, S.W. Joo, O. Manca, An effect of velocity slip and MHD on Hiemenz stagnation flow of ternary nanofluid with heat and mass transfer, *J. Therm. Anal. Calorim.* (2024), https://doi.org/10.1007/s10973-024-12962-7.
[7] Z. Hussain, M. Ayaz, S. Islam, Effects of thermophoresis and Brownian motion on radiative MHD hybrid nanofluid flow over a stretching sheet with convective boundary conditions: a homotopic approach, Proc. Inst. Mech. Eng. Part N: J. Nanomater. Nanoeng. Nanosyst. (2024) 23977914231225019, https://doi.org/10.1177/23977914231225019.
[8] E.M. Elsaid, M.S. Abdel-wahed, MHD mixed convection Ferro Fe_3O_4/Cu-hybrid-nanofluid runs in a vertical channel, Chin. J. Phys. 76 (Mar. 2022) 269–282, https://doi.org/10.1016/j.cjph.2021.12.016.
[9] S.M. Sachhin, U.S. Mahabaleshwar, H.-N. Huang, B. Sunden, D. Zeidan, An influence of temperature jump and Navier's slip-on hybrid nano fluid flow over a permeable stretching/shrinking sheet with heat transfer and inclined MHD, *Nanotechnology* 35 (11) (Dec. 2023) 115401, https://doi.org/10.1088/1361-6528/ad13be.
[10] M.Z. Ahmed, V. Dhanalaxmi, S. Panda, Thermal analysis on Ferro Casson nanofluid flow over a Riga plate with thermal radiation and non-uniform heat source/sink, Mod. Phys. Lett. B (2024) 2450460, https://doi.org/10.1142/S0217984924504608.
[11] S.M. Sachhin, U.S. Mahabaleshwar, D. Zeidan, S.W. Joo, O. Manca, An effect of velocity slip and MHD on Hiemenz stagnation flow of ternary nanofluid with heat and mass transfer, *J. Therm. Anal. Calorim.* (Mar. 2024), https://doi.org/10.1007/s10973-024-12962-7.
[12] M.R. Sohel, R. Saidur, N.H. Hassan, M.M. Elias, S.S. Khaleduzzaman, I. M. Mahbubul, Analysis of entropy generation using nanofluid flow through the circular microchannel and minichannel heat sink, Int. Commun. Heat Mass Transfer 46 (Aug. 2013) 85–91, https://doi.org/10.1016/j.icheatmasstransfer.2013.05.011.
[13] U.S. Mahabaleshwar, S.M. Sachin, A.B. Vishalakshi, G. Bognar, B.A. Sunden, Linear stability analysis of micropolar nanofluid flow across the accelerated surface with inclined magnetic field, *Int. J. Numer. Meth. Heat Fluid Flow* 34 (9) (Jan. 2024) 3515–3541, https://doi.org/10.1108/HFF-05-2024-0372.
[14] G. Huminic, A. Huminic, Entropy generation of nanofluid and hybrid nanofluid flow in thermal systems: A review, J. Mol. Liq. 302 (Mar. 2020) 112533, https://doi.org/10.1016/j.molliq.2020.112533.

[15] A. Hajatzadeh Pordanjani, S. Aghakhani, A. Karimipour, M. Afrand, M. Goodarzi, Investigation of free convection heat transfer and entropy generation of nanofluid flow inside a cavity affected by magnetic field and thermal radiation, J. Therm. Anal. Calorim. 137 (3) (2019) 997–1019, https://doi.org/10.1007/s10973-018-7982-4.
[16] S. Alqaed, J. Mustafa, H.Ş. Aybar, B. Jamil, M.A. Alharthi, Investigation of thermal entropy generation and nanofluid flow in a new heatsink with effect of nanoparticles shape, Case Stud. Therm. Eng. 36 (Aug. 2022) 102198, https://doi.org/10.1016/j.csite.2022.102198.
[17] B. Darbari, S. Rashidi, J. Abolfazli Esfahani, Sensitivity analysis of entropy generation in nanofluid flow inside a channel by response surface methodology, Art. no. 2, Entropy 18 (2) (2016), https://doi.org/10.3390/e18020052.
[18] R.N. Kumar, F. Gamaoun, A. Abdulrahman, J.S. Chohan, R.J.P. Gowda, Heat transfer analysis in three-dimensional unsteady magnetic fluid flow of water-based ternary hybrid nanofluid conveying three various shaped nanoparticles: A comparative study, Int. J. Mod. Phys. B 36 (25) (Oct. 2022) 2250170, https://doi.org/10.1142/S0217979222501703.
[19] O. Pourmehran, M. Rahimi-Gorji, D.D. Ganji, Heat transfer and flow analysis of nanofluid flow induced by a stretching sheet in the presence of an external magnetic field, J. Taiwan Inst. Chem. Eng. 65 (Aug. 2016) 162–171, https://doi.org/10.1016/j.jtice:2016.04.035.
[20] A. Hamid, A. Hashim, A. Hafeez, M. Khan, A.S. Alshomrani, M. Alghamdi, Heat transport features of magnetic water–graphene oxide nanofluid flow with thermal radiation: stability test, Eur. J. Mech. B Fluids 76 (2019) 434–441, https://doi.org/10.1016/j.euromechflu.2019.04.008.
[21] S.M. Sachhin, U.S. Mahabaleshwar, D. Laroze, D. Drikakis, Darcy–Brinkman model for ternary dusty nanofluid flow across stretching/shrinking surface with suction/injection, Art. no. 4, *Fluids* 9 (4) (2024), https://doi.org/10.3390/fluids9040094.
[22] H.R. Ashorynejad, M. Sheikholeslami, I. Pop, D.D. Ganji, Nanofluid flow and heat transfer due to a stretching cylinder in the presence of magnetic field, Heat Mass Transf. 49 (3) (Mar. 2013) 427–436, https://doi.org/10.1007/s00231-012-1087-6.
[23] M. Sheikholeslami, M. Hatami, D.D. Ganji, Nanofluid flow and heat transfer in a rotating system in the presence of a magnetic field, J. Mol. Liq. 190 (Feb. 2014) 112–120, https://doi.org/10.1016/j.molliq.2013.11.002.
[24] N. Sher Akbar, A. Ebaid, Z.H. Khan, Numerical analysis of magnetic field effects on Eyring-Powell fluid flow towards a stretching sheet, *J. Magn. Magn. Mater.* 382 (May 2015) 355–358, https://doi.org/10.1016/j.jmmm.2015.01.088.
[25] Z. Abdelmalek, A. Hussain, S. Bilal, E.-S.-M. Sherif, P. Thounthong, Brownian motion and thermophoretic diffusion influence on thermophysical aspects of electrically conducting viscoinelastic nanofluid flow over a stretched surface, *J. Mater. Res. Technol.* 9 (5) (Sep. 2020) 11948–11957, https://doi.org/10.1016/j.jmrt.2020.08.014.
[26] M. Fathizadeh, M. Madani, Y. Khan, N. Faraz, A. Yıldırım, S. Tutkun, An effective modification of the homotopy perturbation method for MHD viscous flow over a stretching sheet, *J. King Saud Univ. – Sci.* 25 (2) (Apr. 2013) 107–113, https://doi.org/10.1016/j.jksus.2011.08.003.
[27] J.C. Umavathi, O. Ojjela, K. Vajravelu, Numerical analysis of natural convective flow and heat transfer of nanofluids in a vertical rectangular duct using Darcy-Forchheimer-Brinkman model, Int. J. Therm. Sci. 111 (Jan. 2017) 511–524, https://doi.org/10.1016/j.ijthermalsci.2016.10.002.
[28] A. Malvandi, D.D. Ganji, Brownian motion and thermophoresis effects on slip flow of alumina/water nanofluid inside a circular microchannel in the presence of a magnetic field, Int. J. Therm. Sci. 84 (Oct. 2014) 196–206, https://doi.org/10.1016/j.ijthermalsci.2014.05.013.
[29] S. Abelman, A.B. Parsa, H.-O. Sayehvand, Nanofluid flow and heat transfer in a Brinkman porous channel with variable porosity, Quaest. Math. 41 (4) (May 2018) 449–467, https://doi.org/10.2989/16073606.2017.1404503.
[30] M. Sheikholeslami, H.B. Rokni, Magnetic nanofluid flow and convective heat transfer in a porous cavity considering Brownian motion effects, Phys. Fluids 30 (1) (Jan. 2018) 012003, https://doi.org/10.1063/1.5012517.
[31] Z. Shah, T. Gul, S. Islam, M.A. Khan, E. Bonyah, F. Hussain, S. Mukhtar, M. Ullah, Three-dimensional third grade nanofluid flow in a rotating system between parallel plates with Brownian motion and thermophoresis effects, Results Phys. 10 (Sep. 2018) 36–45, https://doi.org/10.1016/j.rinp.2018.05.020.
[32] J.K. Singh, G.S. Seth, S.M. Hussain, Thermal performance of hydromagnetic nanofluid flow within an asymmetric channel with arbitrarily conductive walls filled with Darcy-Brinkman porous medium, J. Magn. Magn. Mater. 582 (Sep. 2023) 171034, https://doi.org/10.1016/j.jmmm.2023.171034.
[33] J.V. Tawade, C.N. Guled, S. Noeiaghdam, U. Fernandez-Gamiz, V. Govindan, S. Balamuralitharan, Effects of thermophoresis and Brownian motion for thermal and chemically reacting Casson nanofluid flow over a linearly stretching sheet, Results Eng. 15 (Sep. 2022) 100448, https://doi.org/10.1016/j.rineng.2022.100448.
[34] W.I. Liu, J. Alsarraf, A. Shahsavar, M. Rostamzadeh, M. Afrand, T.K. Nguyen, Impact of oscillating magnetic field on the thermal-conductivity of water-Fe3O4 and water-Fe3O4/CNT ferro-fluids: Experimental study, J. Magn. Magn. Mater. 484 (Aug. 2019) 258–265, https://doi.org/10.1016/j.jmmm.2019.04.042.
[35] J. Yang, Z. Abdelmalek, N. Muhammad, M.T. Mustafa, Hydrodynamics and ferrite nanoparticles in hybrid nanofluid, Int. Commun. Heat Mass Transfer 118 (Nov. 2020) 104883, https://doi.org/10.1016/j.icheatmasstransfer.2020.104883.
[36] Y.-J. Xu, F. Shah, M.I. Khan, R. Naveen Kumar, R.J. Punith Gowda, B. C. Prasannakumara, M.Y. Malik, S.U. Khan, New modeling and analytical solution of fourth grade (non-Newtonian) fluid by a stretchable magnetized Riga device, *Int. J. Mod. Phys. C* 33 (01) (2022) 2250013, https://doi.org/10.1142/S0129183122500139.
[37] M.I. Khan, S. Kadry, Y. Chu, M. Waqas, Modeling and numerical analysis of nanoliquid (titanium oxide, graphene oxide) flow viscous fluid with second order velocity slip and entropy generation, *Chin. J. Chem. Eng.* 31 (Mar. 2021) 17–25, https://doi.org/10.1016/j.cjche.2020.08.005.
[38] M. Nazeer, M.I. Khan, Y.-M. Chu, S. Kadry, M.R. Eid, Mathematical modeling of multiphase flows of third-grade fluid with lubrication effects through an inclined channel: analytical treatment, *J. Dispers. Sci. Technol.* 43 (10) (Aug. 2022) 1555–1567, https://doi.org/10.1080/01932691.2021.1877557.
[39] W.-M. Qian, M.I. Khan, F. Shah, M. Khan, Y.M. Chu, W.A. Khan, M. Nazeer, Mathematical modeling and MHD flow of micropolar fluid toward an exponential curved surface: heat analysis via ohmic heating and heat source/sink, *Arab. J. Sci. Eng.* 47 (1) (Jan. 2022) 867–878, https://doi.org/10.1007/s13369-021-05673-w.
[40] M.I. Khan, F. Shah, S.U. Khan, A. Ghaffari, Y.M. Chu, Heat and mass transfer analysis for bioconvective flow of Eyring Powell nanofluid over a Riga surface with nonlinear thermal features, *Numer. Methods Partial Differ. Equ.* 38 (4) (2022) 777–793, https://doi.org/10.1002/num.22696.
[41] B. Guo, A. Raza, K. Al-Khaled, S.U. Khan, S. Farid, Y. Wang, M.I. Khan, M.Y. Malik, S. Saleem, Fractional-order simulations for heat and mass transfer analysis confined by elliptic inclined plate with slip effects: A comparative fractional analysis, *Case Stud. Therm. Eng.* 28 (Dec. 2021) 101359, https://doi.org/10.1016/j.csite.2021.101359.
[42] S. Das, R.R. Patra, R.N. Jana, The layout of Boussinesq couple-stress fluid flow over an exponentially stretching sheet with slip in porous space subject to a variable magnetic field, *Multidiscip. Model. Mater. Struct.* 16 (5) (May 2020) 1131–1154, https://doi.org/10.1108/MMMS-09-2019-0168.
[43] S. Das, A. Ali, R.N. Jana, Darcy–Forchheimer flow of a magneto-radiated couple stress fluid over an inclined exponentially stretching surface with Ohmic dissipation, *World J. Eng.* 18 (2) (Dec. 2020) 345–360, https://doi.org/10.1108/WJE-07-2020-0258.
[44] A. Ali, R.N. Jana, S. Das, Radiative CNT-based hybrid magneto-nanoliquid flow over an extending curved surface with slippage and convective heating, *Heat Transf.* 50 (3) (2021) 2997–3020, https://doi.org/10.1002/htj.22015.
[45] A. Ali, R.N. Jana, S. Das, Hall effects on radiated magneto-power-law fluid flow over a stretching surface with power-law velocity slip effect, *Multidiscip. Model. Mater. Struct.* 17 (1) (Jun. 2020) 103–125, https://doi.org/10.1108/MMMS-01-2020-0005.
[46] R. Adhikari, S. Das, Biological transmission in a magnetized reactive Casson–Maxwell nanofluid over a tilted stretchy cylinder in an entropy framework, *Chin. J. Phys.* 86 (Dec. 2023) 194–226, https://doi.org/10.1016/j.cjph.2023.10.008.
[47] P. Karmakar, S. Das, N. Mahato, A. Ali, R.N. Jana, Dynamics prediction using an artificial neural network for a weakly conductive ionized fluid streamed over a vibrating electromagnetic plate, *Eur. Phys. J. Plus* 139 (5) (May 2024) 407, https://doi.org/10.1140/epjp/s13360-024-05197-w.
[48] D. Yadav, J. Wang, R. Bhargava, J. Lee, H.H. Cho, Numerical investigation of the effect of magnetic field on the onset of nanofluid convection, Appl. Therm. Eng. 103 (2016) 1441–1449.
[49] D. Yadav, J. Wang, Convective heat transport in a heat generating porous layer saturated by a non-Newtonian nanofluid, Heat Transfer Eng. 40 (16) (2019) 1363–1382.
[50] N. Alipour, B. Jafari, K. Hosseinzadeh, Thermal analysis and optimization approach for ternary nanofluid flow in a novel porous cavity by considering nanoparticle shape factor, *Heliyon* 9 (12) (Dec. 2023), https://doi.org/10.1016/j.heliyon.2023.e22257 e22257.
[51] N. Alipour, B. Jafari, K. Hosseinzadeh, Analysis of the impact of metal foam with phase change material on solar photovoltaic thermal system efficiency, *J. Energy Storage* 98 (Sep. 2024) 113064, https://doi.org/10.1016/j.est.2024.113064.
[52] S. Akbari, M.F. Farahani, K. Hosseinzadeh, Theoretical analysis of transient counter-flow combustion system fueled by porous biomass particles in a non-premixed configuration under non-adiabatic conditions, *Int. J. Thermofluids* 22 (May 2024) 100653, https://doi.org/10.1016/j.ijft.2024.100653.
[53] M.S. Kausar, M. Waqas, S.A. Shehzad, Kh. Hosseinzadeh, H.A. Hejazi, W. Mtaouaa, Numerical computations for Darcy–Forchheimer-based dual convection reactive flow considering Casson nanomaterial by convected permeable surface, *Int. J. Mod. Phys. B* 38 (31) (Dec. 2024) 2450426, https://doi.org/10.1142/S0217979224504265.
[54] D. Yadav, M.K. Awasthi, R. Ragoju, K. Bhattacharyya, R. Kodi, J. Wang, The impact of rotation on the onset of cellular convective movement in a casson fluid saturated permeable layer with temperature dependent thermal conductivity and viscosity deviations, Chin. J. Phys. 91 (2024) 262–277.
[55] M.R. Zangooee, K. Hosseinzadeh, D.D. Ganj, Investigation of three-dimensional hybrid nanofluid flow affected by nonuniform MHD over exponential stretching/shrinking plate, *Nonlinear Eng.* 11 (1) (Jan. 2022) 143–155, https://doi.org/10.1515/nleng-2022-0019.
[56] S.M. Moghimi, K. Hosseinzadeh, A. Hasibi, Investigation of nanofluid flow in the channel under effect of magnetic field and joule heating, *Case Stud. Therm. Eng.* 55 (Mar. 2024) 104152, https://doi.org/10.1016/j.csite.2024.104152.
[57] M. Mahboobtosi, K. Hosseinzadeh, D.D. Ganji, Investigating the convective flow of ternary hybrid nanofluids and single nanofluids around a stretched cylinder: Parameter analysis and performance enhancement, *Int. J. Thermofluids* 23 (Aug. 2024) 100752, https://doi.org/10.1016/j.ijft.2024.100752.
[58] S. Hosseinzadeh, Kh. Hosseinzadeh, A. Hasibi, D.D. Ganji, Hydrothermal analysis on non-Newtonian nanofluid flow of blood through porous vessels, *Proc. Inst. Mech. Eng. Part E J. Process Mech. Eng.* 236 (4) (2022) 1604–1615, https://doi.org/10.1177/09544089211069211.

[59] M. Farmahini Farahani, S. Akbari, K. Hosseinzadeh, Evaluation of thermal radiation and Lewis number effects on oscillatory thermal-diffusive instabilities of counterflow premixed flame fed with moist biomass particles, *Case Stud. Therm. Eng.* 58 (2024) 104369, https://doi.org/10.1016/j.csite.2024.104369.

[60] A. Najafpour, E. Montazer, K. Hosseinzadeh, A.A. Ranjbar, D.D. Ganji, J. Kanesan, Computational study on the impact of geometric parameters on the overall efficiency of multi-branch channel heat sink in the solar collector, *Int. Commun. Heat Mass Transf.* 158 (Nov. 2024) 107884, https://doi.org/10.1016/j.ic36heatmasstransfer.2024.107884.

[61] A. Jafarimoghaddam, Wall jet flows of Glauert type: Heat transfer characteristics and the thermal instabilities in analytic closed forms, *Eur. J. Mech. B. Fluids* 71 (Sep. 2018) 77–91, https://doi.org/10.1016/j.euromechflu.2018.04.002.

[62] U. Khan, A. Zaib, A. Ishak, Impact of thermal and activation energies on Glauert wall jet (WJ) heat and mass transfer flows induced by ZnO-SAE50 nano lubricants with chemical reaction: the case of Brinkman-extended Darcy model, *Lubricants* 11 (1) (2023) 22, https://doi.org/10.3390/lubricants11010022.

[63] M. Yaseen, et al., Computational analysis of heat and mass transfer flow of wall jet hybrid nanofluid with irregular heat source/sink effects and waste discharge concentration, *J. Magn. Magn. Mater.* 588 (Dec. 2023) 171434, https://doi.org/10.1016/j.jmmm.2023.171434.

[64] M.B. Glauert, The Wall Jet, J. Fluid Mech. 1 (1956) 625–643, https://doi.org/10.1017/S002211205600041X.